Theor Chem Acc (1997) 96:195–204

Theoretical
Chemistry Accounts

The intersection seam between the $1^1A'$ and $2^1A'$ states of ozone

G. J. Atchity, K. Ruedenberg, A. Nanayakkara

Ames Laboratory, US Department of Energy, and Department of Chemistry, Iowa State University, Ames, IA 50011, USA

Received: 10 January 1996 / Accepted: 2 January 1997

Abstract The intersection seam between the two lowest $^1A'$ states of ozone has been determined. The potential energy surfaces and the seam are calculated and discussed in perimetric coordinates which exhibit the full three-dimensional symmetry. The seam is shown to form a closed curve which crosses the C_{2v}-restricted coordinate planes at six points. Three of these correspond to the previously determined intersection, the starting point of the present search. The other three correspond to highly repulsive regions on the potential energy surface where two atoms approach each other to within two-thirds of the O_2 bond length. At the former three points both states have $^1A_1$ symmetry, but at the latter three points one state has $^1A_1$ symmetry whereas the other has $^1B_2$ symmetry. Consequently, there exist three additional branches of the intersection seam between these two states. Each of these branches lies entirely in one C_{2v}-restricted coordinate plane and connects to the previously discussed C_s-seam at one point. The existence of a further intersection seam is established. A novel method for determining intersection points is described.

Key words: Conical intersection – Intersection seam – Diabatic states – Ozone

1 Introduction

In recent investigations [1], we have found that the ground state of ozone has a point of degeneracy, a conical intersection, with the first excited state of like symmetry ($^1A_1$) in the C_{2v}-restricted two-dimensional internal coordinate space between the two ground state minima. We have also identified those features of the electronic structure which are responsible for this somewhat unusual phenomenon [2].

In view of the fundamental theory pertaining to conical intersections [3], it was apparent from the beginning that the point previously found would have to be a point on *a one-dimensional curve* along which the two states remain degenerate in the full three-dimensional internal coordinate space: *an intersection seam between the* $1^1A'$ *and the* $2^1A'$ *states*.

To our knowledge, the only previous determination of *full* intersection seams between surfaces of like symmetry (termed "accidental conical intersections" by the authors) is by Kuntz et al. who investigated the H_2Cl^+ system in beautiful detail [4]. Therefore, it seemed of general interest to map out this particular seam rather carefully in the full internal coordinate space of C_s symmetry. It was also an intriguing question whether the seam would be a closed curve or move out toward the dissociated species without closing.

In what follows we shall describe the methods we developed for following an intersection seam and the characteristics of the seam which was established.

2 Energy functions in terms of perimetric coordinates

2.1 Coordinate space

For the present investigation, it is essential that all three nuclei be treated on an equal footing. To this end, we shall use *perimetric coordinates* which have been previously used by James and Coolidge [5], Pekeris [6], and Davidson [7]. We discuss relevant elements of these coordinates in some detail in a companion paper [8].

If r_{12}, r_{23}, r_{31} are the three internuclear distances, then the perimetric coordinates s_1, s_2, s_3 are defined by the formulas

$$r = r_{12} + r_{23} + r_{31}, \tag{1}$$

$$s_i + r_{jk} = s = r/2, \tag{2}$$

$$s = s_1 + s_2 + s_3. \tag{3}$$

They can be separated into the scale coordinate s and the angle-dependent, but scale-independent shape coordinates ξ_1, ξ_2 which are related to (s_1 s_2, s_3) by

$$\begin{aligned} s_1 &= s\{-\xi_1/\sqrt{2} - \xi_2/\sqrt{6} + 1/3\} \\ s_2 &= s\{\xi_1/\sqrt{2} - \xi_2/\sqrt{6} + 1/3\} \\ s_3 &= s\{2/\sqrt{6} + 1/3\} \end{aligned} \tag{4}$$

Correspondence to: K. Ruedenberg

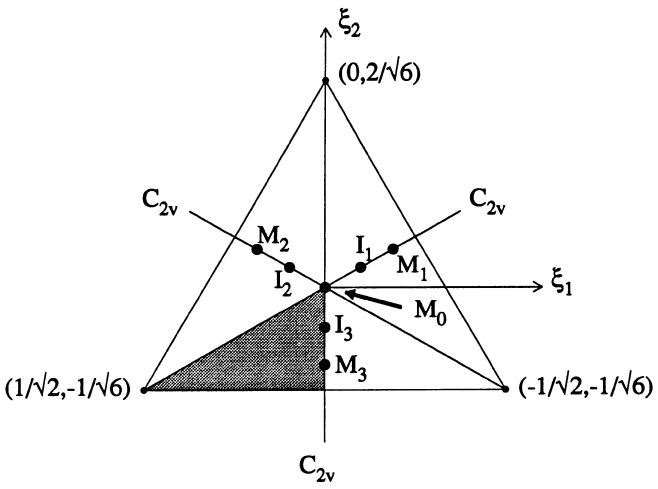

Fig. 1. Parameter space of the scale-independent shape coordinates. The labelled points are defined in Section 3.1

The parameter space of the shape coordinates $(\xi_1,\ \xi_2)$ covers an equilateral triangle whose dimensions are displayed in Fig. 1, where some special points and regions are indicated as well. Also useful are the coordinates

$$x_1 = s\xi_1, \qquad x_2 = s\xi_2, \qquad x_3 = s/\sqrt{3} \tag{5}$$

which, by virtue of Eq. (4), are related to $(s_1,\ s_2,\ s_3)$ through an orthogonal transformation that places the x_3 axis along the first-octant diagonal of the $s_1,\ s_2,\ s_3$ axis system. In order to fully appreciate and visualize the meaning of these coordinates, the reader should consult the explicit discussion in reference [8] which also clarifies the following statements.

When the shape coordinates fall on one of the perpendiculars from one corner of the triangle in Fig. 1, through the center, on to the opposite side, then two internuclear distances are equal and this remains true in the entire plane spanned by this perpendicular line and the x_3 axis. For example, for all points with $\xi_1 = 0$, be they on the ξ_2 axis in Fig. 1 or in the plane spanned by x_2 and x_3, the molecule is isosceles, with nucleus 3 at the apex. The center point, $\xi_1 = \xi_2 = 0$, as well as all points on the x_3 axis, correspond to equilateral molecules.

Two points in the shape-coordinate triangle, which are related to each other by reflection with respect to the perpendicular from corner (*i*) in Fig. 1 to the opposite side (*j*-*k*), describe two molecules which are obtained from each other by permuting atoms *j* and *k*, and, hence, their shapes are each other's mirror images with respect to any reflection plane normal to the line connecting nuclei *j* and *k*.

2.2 Energy surfaces for homonuclear triatomic molecules

Since ozone is a homonuclear molecule, its potential energy surface (PES) must be invariant with respect to all permutations of its nuclei. By virtue of what has been said in the preceding section, it is readily seen that this invariance implies the invariance of the potential energy surfaces with respect to the symmetry operation of the group C_{3v}, *if applied in the parameter space of the perimetric coordinates*, with the C_3 axis along the x_3 coordinate axis and the three planes of symmetry being the planes spanned by the x_3 axis and the normals from the corners of the shape-coordinate triangle of Fig. 1 to the opposite sides. Each PES can therefore be generated from its values in one-sixth of the entire coordinate space. The projection of this part onto the shape coordinate plane is shaded in Fig. 1. It follows, furthermore, that the planes spanned by the x_3 axis and the normals from the corners of the coordinate triangle of Fig. 1 to the opposite sides, i.e. the symmetry planes of C_{3v} in the parameter space, contain the coordinates of all those molecules which possess C_{2v} symmetry. We shall therefore call these planes the C_{2v}-restricted coordinate spaces. The x_3 axis, i.e. the C_3 axis of C_{3v} in parameter space, corresponds to all molecules with D_{3h} symmetry.

The intersection seam is a curve in the three-dimensional coordinate space. Since it runs on potential energy surfaces, it too is invariant under the operations of C_{3v} in the parameter space and it, too, can be generated in full after one-sixth of it has been found. It also follows from this symmetry that such a seam must penetrate each of the symmetry planes of the C_{3v} group in the parameter space at right angles.

We shall display the intersection seam by exhibiting (1) a plot of its projection in the (ξ_1, ξ_2) plane inside the triangle of Fig. 1, (2) a plot graphing the variation of $s = x_3\sqrt{3}$ along the just mentioned projection curve, and (3) a plot of the intersection energy(E) along the same curve. By virtue of the discussed symmetry properties, the projection in the (ξ_1, ξ_2) plane must perpendicularly cross the normals from the corners of the triangle in Fig. 1 onto the opposite sides, and the plots of *s* and E must have horizontal slopes at the points of crossing these C_{2v}-restricted coordinate spaces. These symmetry properties apply regardless of whether the intersection seam is a closed or an open curve.

3 Determination of the seam

3.1 Point to point extrapolation

In previous investigations [1, 2] we established the intersection point in C_{2v} symmetry. Because of the threefold symmetry of the PES, this result yields in fact three intersection points in the coordinate space, which are shown in Fig. 1 as I_1, I_2, I_3. Also shown are the positions of the four minima M_0, M_1, M_2, M_3. The x_3 coordinates, which are not shown, are given by the scale parameters with the values

$$s(I_i) \ = 2.456\text{Å}, \quad s(M_0) = 2.214\text{Å},$$
$$s(M_i) = 2.412\text{Å}, \quad (i = 1, 2, 3).$$

We started the determination of the intersection seam at the point I_3, which has the coordinates

$$x_1^{(0)} = 0, \qquad x_2^{(0)} = -0.392\text{Å}, \qquad x_3^{(0)} = 1.418\text{Å}.$$

Since, as explained above, the seam must cross the $x_2 - x_3$ plane at a right angle, a reasonable first guess for the next point on the seam is

$$x_1^{(1)} = \varepsilon, \qquad x_2^{(1)} \approx x_2^{(0)}, \qquad x_3^{(1)} \approx x_3^{(0)},$$

and a reasonable search surface for the *exact* next seam point is the plane $x_1^{(1)} = \varepsilon = \text{constant}$. A search, to be described below, on this plane around the predicted guess yielded then the actual intersection point $(x_1^{(1)} = \varepsilon, x_2^{(1)}, x_3^{(1)})$. Because of the symmetry of the seam with respect to the plane $x_1 = 0$, this calculation also yielded a third intersection point, namely:

$$x_1^{(-1)} = -\varepsilon, \qquad x_2^{(-1)} = x_2^{(1)}, \qquad x_3^{(-1)} = x_3^{(1)}.$$

From here on, the initial guess for each additional seam point was determined by a quadratic extrapolation from the preceding three seam points. The coefficients a to f in the expressions

$$x_2 = a + bx_1 + cx_1^2$$
$$x_3 = d + ex_1 + fx_1^2$$

were determined by a fit to the points $(n), (\mathrm{n}-1), (n-2)$ of the seam and then used to predict the values of $x_2^{(n+1)}$ and $x_3^{(n+1)}$ for $x_1^{(n+1)} = x_1^{(n)} + \varepsilon$. The *exact* values of $x_2^{(n+1)}$ and $x_3^{(n+1)}$ were then again determined by searching for the intersection point in the plane $x_1^{(n+1)} = x_1^{(n)} + \varepsilon = \text{constant}$.

Approximately the same value of about $\varepsilon \approx 0.02$ Å was used for the increments at the various points, unless difficulty was encountered. We were prepared to change the extrapolation variable from x_1 to some linear combination of x_1, x_2, x_3, and, correspondingly, the choice of the search plane, in the event that the intersection seam should curve away significantly from the x_1 direction. Such a change proved, however, unnecessary because the seam was found to stay closely parallel to the x_1 axis.

Since the completion of this work, Kuntz et al. have shown [4] that a more reliable and efficient choice is to construct the search plane at each point perpendicular to the [$(N-2)$ dimensional] intersection seam.

While the initial point of the seam corresponds to a molecule with C_{2v} symmetry, the molecular symmetry is lowered to C_s for the new points on the seam, so that the calculations involve more work. However, after having passed through the shaded region of Fig. 1, the seam reaches again a point where the molecule has C_{2v} symmetry. This end-point can therefore be rechecked by an independent calculation using C_{2v} symmetry.

3.2 Planar search by minimizing $(E_2 - E_1)^2$

Because of the conical nature of the intersection [3], the difference between the two potential energy surfaces, $(E_2 - E_1)$, cannot be fit by a quadratic, but its square, $(\Delta E)^2$, can. We therefore calculated E_1 and E_2 on each plane $x_1 = \text{constant}$ for a grid around the initial guess, fit a quadratic to the $(\Delta E)^2$ values on this grid, determined the minimum, recalculated E_1 and E_2 on a finer grid around this minimum, and proceeded in the same manner until the energy separation at the minimum was reduced to less then half a microhartree.

This procedure, which is analogous to the one used in our previous work [1] to determine the initial point I_3, proved quite straightforward. It is not overly efficient regarding the number of energy calculations needed and can be considerably improved by using a quasi-Newton procedure with the analytical derivatives, as Manaa and Yarkony [9] have shown. More sophisticated search procedures, based on Lagrangian formalisms using the derivatives of $(H_{11} - H_{22})$ and H_{12}, have been developed by Manaa and Yarkony [10] and by Ragazos et al. [11].

However, none of these procedures can prove conclusively that the two surfaces in fact do become *exactly* degenerate. This shortcoming is overcome by the following approach.

3.3 Corralling an intersection point

According to the Herzberg–Longuet-Higgins–Berry phase theorem [3], wave functions Ψ_1 and Ψ_2 both change sign when deformed continuously on a closed path looping around an intersection. In our previous investigation [1], we used this theorem as a test to prove the existence of a true intersection between the two 1^1A_1 states in C_{2v}: if there were no true intersection, neither function would change sign. We shall now show how this approach can be adapted for the accurate determination of the location of an intersection once its approximate position is known.

An obvious approach is as follows. First, calculate Ψ_1 and Ψ_2 on a closed path around the suspected point of intersection. If the wave functions do not change sign, find another guess of the intersection until the wave functions do change sign. Next calculate Ψ_1 and Ψ_2 along a line connecting opposite sides of the loop, thereby in effect creating two loops each containing about half the area of the original loop. One of the two loops created will contain the intersection and, hence, exhibit the sign changes in Ψ_1 and Ψ_2. The other will not. Then, proceed to cut the loop with the intersection in half and repeat the procedure. Successive repetitions of this bisection will decrease the size of the loops until the desired accuracy is reached.

This approach can, however, be considerably refined by a closer analysis of the phase change. It is known [3] that the adiabatic states Ψ_1, Ψ_2 can be expressed in terms of two diabatic states ϕ_1, ϕ_2 by the orthogonal transformation

$$\begin{aligned} \Psi_1 &= \phi_1 \cos(\alpha/2) \;+\; \phi_2 \sin(\alpha/2) \\ \Psi_2 &= -\phi_1 \sin(\alpha/2) \;+\; \phi_2 \cos(\alpha/2), \end{aligned} \tag{6}$$

where the angle α is obtained from the diabatic matrix elements $H_{ij} = \langle \phi_i | H | \phi_j \rangle$ and $\Delta H = H_{11} - H_{22}$, by the equations

$$\cos(\alpha) = \Delta H / (\Delta H^2 + H_{12}^2)^{1/2} \tag{7}$$

$$\sin(\alpha) = H_{12} / (\Delta H^2 + H_{12}^2)^{1/2} \tag{8}$$

An intersection occurs when ΔH and H_{12} both change signs [3]. Figure 2 exhibits a schematic diagram of the coordinate space near an intersection. The difference ΔH changes sign along the curve $\Delta H = 0$, the off-diagonal element H_{12} changes sign along the curve $H_{12} = 0$. Also shown is a closed path looping around the intersection of these two curves, which is, in fact, the point of degeneracy between the two energy surfaces.

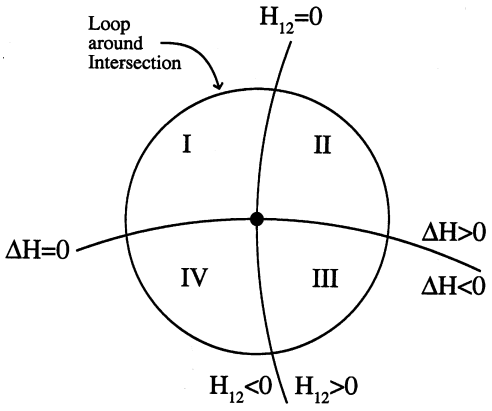

Fig. 2. The four regions generated by the surfaces $\Delta H = 0$ and $H_{12} = 0$ around an intersection. The latter is indicated by the *heavy dot*

It follows from Eq. (7) that, in regions I and II, the diabatic state ϕ_1 dominates in the adiabatic state Ψ_1, and that the diabatic state ϕ_2 dominates in the adiabatic state Ψ_2, whereas the reverse is true in regions III and IV. Concomitantly, $\Delta H = 0$ is a line of avoided crossings, except that at the intersection one has a real crossing. Consequently, one observes a *change-over in the dominant configurations* in Ψ_1 and Ψ_2 along the closed path *whenever it crosses the curve* $\Delta H = 0$. On the other hand, it also follows from Eqs. (6), (7), and (8) that the *small coefficients* in the adiabatic states, i.e. the coefficients of those configurations which are *not* dominant in Ψ_1 and Ψ_2, change sign where H_{12} changes sign, i.e. *whenever the path crosses the curve* $H_{12} = 0$. We have noted these connections explicitly in a previous paper [2].

By virtue of these relationships, the overall sign change in the wave function Ψ_1, say, comes about as a result of the individual changes illustrated in Fig. 3 when moving around the loop. By careful monitoring of the major and the minor configurations, it is therefore possible to obtain an approximate idea where the loop around the intersection crosses the lines $\Delta H = 0$ and $H_{12} = 0$. The intersection of the lines connecting these opposite points on the loop will then yield an approximation to the intersection.

The case at hand is a particularly favorable one since all dominant configurations in the adiabatic states Ψ_1 and Ψ_2 contain doubly occupied orbitals only and, hence, also for the diabatic states ϕ_1, ϕ_2. Consequently,

	Region I	Region II	Region III	Region IV	Region I
Coeffs. of ϕ_1 in ψ_1	Large	Large	Small	-Small	-Large
Coeffs. of ϕ_2 in ψ_1	Small	-Small	-Large	-Large	-Small
		$H_{12}=0$	$\Delta H=0$	$H_{12}=0$	$\Delta H=0$

Fig. 3. Illustration of adiabatic wavefunction sign change about intersection

the sign changes of the coefficients of the diabatic states in the adiabatic wave functions are reflected by the sign changes in *the coefficients of the dominant configurations in the adiabatic states* [1] and, hence, are easy to spot.

The method is illustrated in Fig. 4 for the determination of the intersection point in C_{2v} symmetry. The

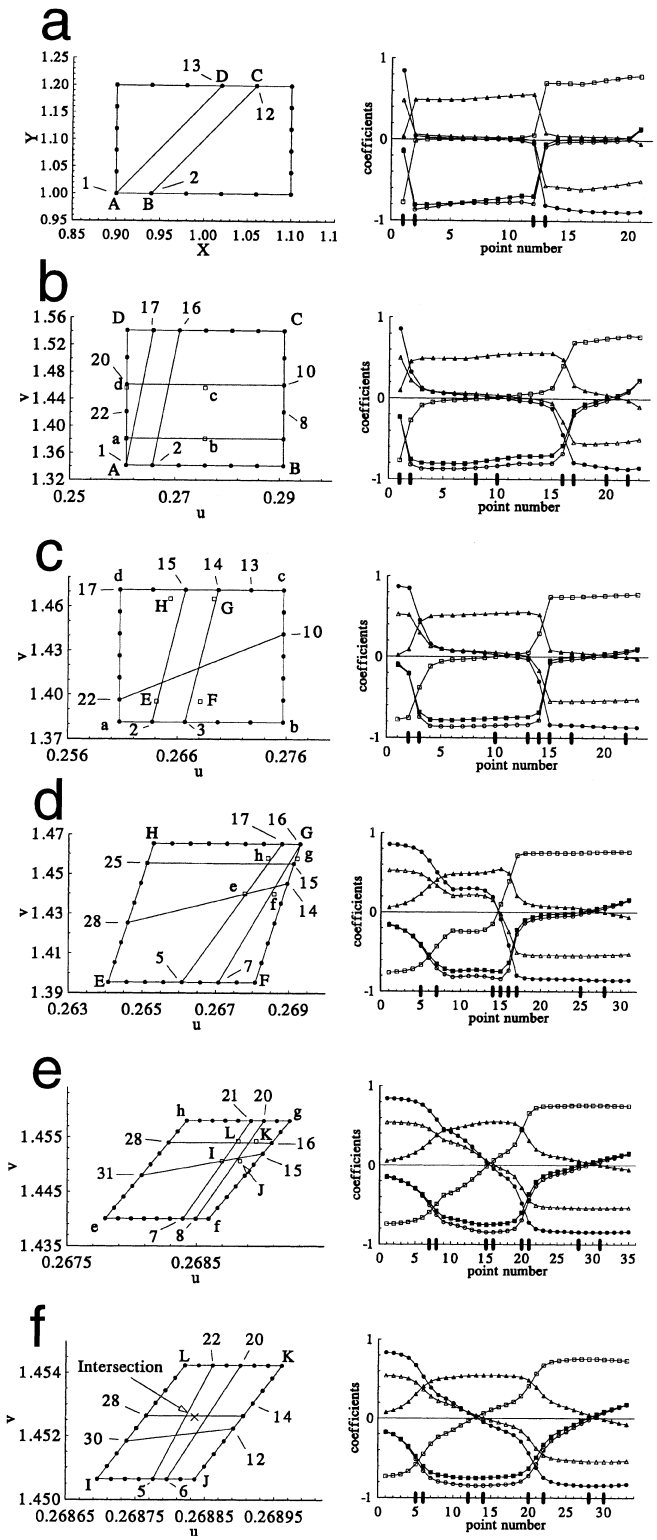

Fig. 4. Corralling an intersection. See text

left-hand panels of each figure display increasingly smaller paths in coordinate space looping around the intersection point in C_{2v} symmetry. Each loop has the shape of a rectangle or parallelogram. The coordinates x, y in the left-hand panel of Fig. 4a are the Cartesian internal coordinates used previously (Fig. 3 of Ref.[1]), while the coordinates u, v on the left-hand panels of Figs. 4b and 4c have been rotated by 31° with respect to x, y. In Fig. 4d, the coordinates of the left panel have been rotated by 32° and those of Figs. 4e and 4f were rotated by 33° with respect to x, y. The solid dots on the loop in each left-hand panel mark the points on the path where wave functions were calculated.

The right-hand panels show the values of the coefficients of the three configurations which are dominant in one state or the other, calculated at the points marked on the loops at left. The abscissa of each panel at right simply numbers these points sequentially. From the preceding discussion it follows that, in the regions where the large coefficients exchange dominance with the small ones, a loop must cross the line $\Delta H = 0$, whereas, in the regions where the small coefficients change sign, the crossing of a loop with the line $H_{12} = 0$ must occur. The boundaries of these crossings are marked by pairs of small bold tick marks on the abscissas of the right panels (with generous room for error). The points corresponding to these tick marks are indicated on the loops of the corresponding panels on the left by explicit numbering. (e.g. 5, 7, 14, 15, 16, 17, 25, 28 on the left panel of Fig. 4a). These points, on opposite parts of the loop, are connected by straight lines. The lines going more or less vertically are expected to bracket the curve $\Delta H = 0$, whereas the lines going more or less horizontally are expected to bracket the curve $H_{12} = 0$. Guided by these lines, the corners for a smaller loop are estimated and they are indicated by letters inside each panel. These letters then appear at the corners of the loop on the next panel. In six iterations, the loop has been reduced from a 0.2 Å × 0.2 Å box to a 0.0004 Å × 0.00003 Å box (in the rotated coordinates), whereas, using the divide-by-2 method, six iterations would reduce the size of the box only to $0.02/2^5 = 0.00625$ Å. Various ways exist in which the convergence of this procedure can be accelerated.

4 The intersection seam of the $1^1A'$ and the $2^1A'$ states

4.1 Ab-initio procedure

The entire intersection seam of the two lowest $^1A'$ states of ozone in C_s symmetry was determined using two-state-averaged Full Optimized Reaction Space (FORS) wave functions, in the full active space generated by all 2p orbitals on all three oxygen atoms, giving 1292 configurations of symmetry C_s. The two states were given equal weight in the averaging. The basis set was of the generally contracted double-zeta type, viz., (11s6p1d/3s2p1d). The s and p exponents were taken from Dunning's VQZ basis set [12]. The 1s, 2s, and 2p contractions were the self-consistent field (SCF) orbitals, while the 3s and 3p orbitals were simply the most diffuse Gaussians of each set. The d orbital set had an exponent of 1.185, the one used by Dunning in his VDZ basis set. All calculations were made with the program MOLPRO of Werner and Knowles [13].

4.2 The intersection seam in C_s, symmetry

The intersection seam is depicted in Fig. 5 and 6. Figure 5 displays the projection of the seam path on the plane of the shape coordinates ξ_1, ξ_2. The points A through C on Fig. 5 are the uniquely calculated points; the rest of the seam was generated by symmetry. The point marked C is the actual starting point in the calculations. It is the location of the previously reported intersection point I_3 in C_{2v} symmetry, very near the transition point between the two minima on the lower surface (marked M_0 and M_1). *It is apparent from Fig. 5 that the seam is a closed path.* It intersects each of the three C_{2v} lines in two points: the symmetry-related points C, F, H are the originally known points I_1, I_2, I_3; the symmetry-related points A, E, G are new points. Figure 6 shows the variation of the molecular circumference r [related to x_3 according to Eqs. (1) and (5)] along the seam. Figure 7 illustrates the variation of the molecular shape along the seam path. Point C is in the center, with the 116° apex angle of the isosceles molecules at the top. As the molecule moves along the path toward point A the top atom moves down and to the right, closing in on the lower right-hand atom until a new C_{2v} axis appears, now bisecting the two atoms at right. Table 1 lists the bond lengths for the points M_3, M_0, C, and A.

Because of the very short bond length of r_{23} at point A and the correspondingly small bond angle at atom 1

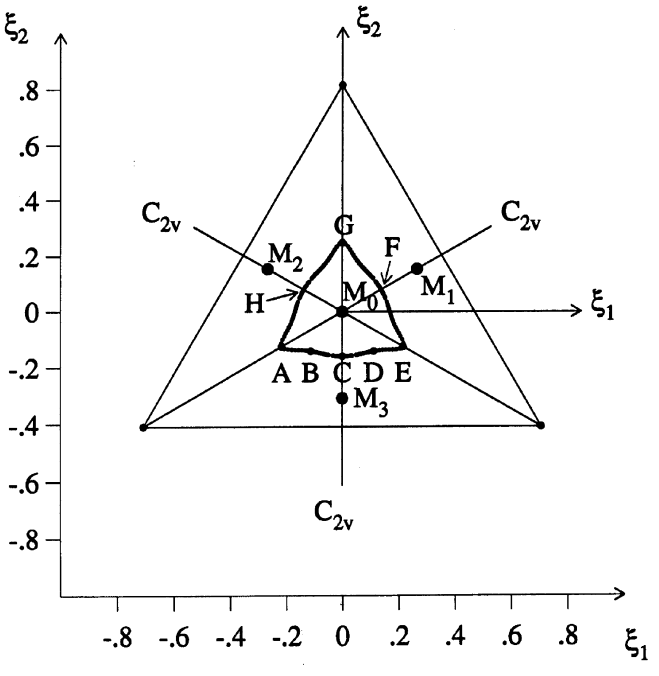

Fig. 5. Projection of the $1^1A'$-$2'A'$ intersection seam of ozone onto the scale-independent shape coordinate space

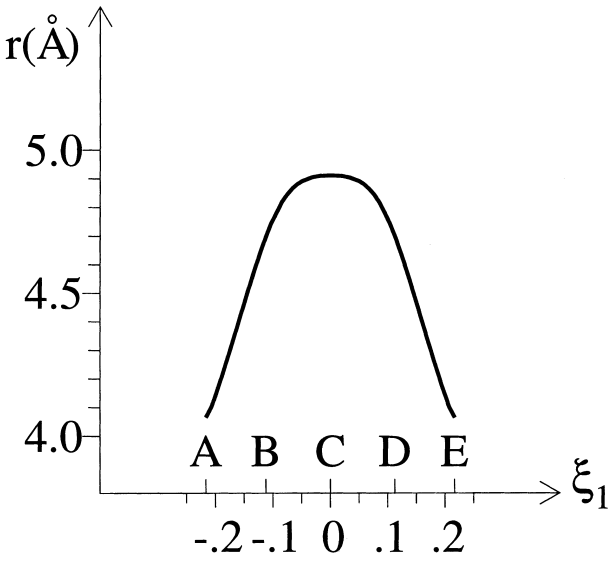

Fig. 6. Variation of the molecular circumference along the intersection seam of Fig. 5

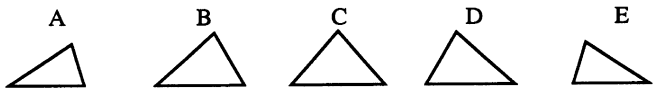

Fig. 7. Variation of the molecular shape along the intersection seam described by Figs. 5 and 6

Table 1 Bond lengths of ozone at various geometries

	r_{13}	r_{23}	r_{12}
Point M_3	1.305	1.305	2.214
Point M_0	1.476	1.476	1.476
Point C	1.477	1.477	1.957
Point A	1.563	0.940	1.563

(about 33.5°), the molecule is obviously very unstable at this geometry. The energy along the seam is displayed in Fig. 8, which confirms that the C_{2v} intersections A, E, G lie in a highly repulsive region of the PES. The repulsive character in the region of point A is also illustrated by Fig. 9, which shows a projection of the intersection seam on the PES contour map for the circumference $r = 4.6$ Å, which is about midway on the seam. Even for this constant value of r, the energy difference between the two different C_{2v} points A and C is about 80 mh. Because of the variation in r, shown in Fig. 6, the difference between points A and C in Fig. 8 is in fact about 370 mh.

The points at which the intersection seam was actually determined are indicated by the dots on the *abscissa* of Fig. 8.

4.3 The intersection seam in C_{2v} symmetry

In C_s symmetry there are two irreps: A′ (symmetric with respect to the molecular plane) and A″ (antisymmetric with respect to the molecular plane). The two irreps of C_{2v}, labeled A_1 and B_2, are compatible with the A′ irrep

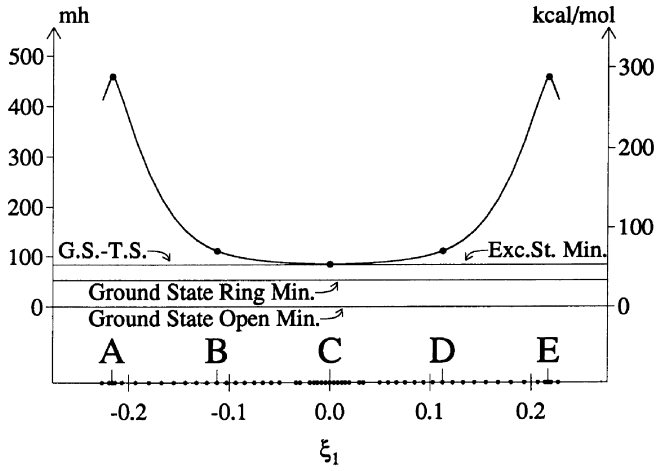

Fig. 8. Variation of the molecular energy along the intersection seam described by Figs. 5 and 6

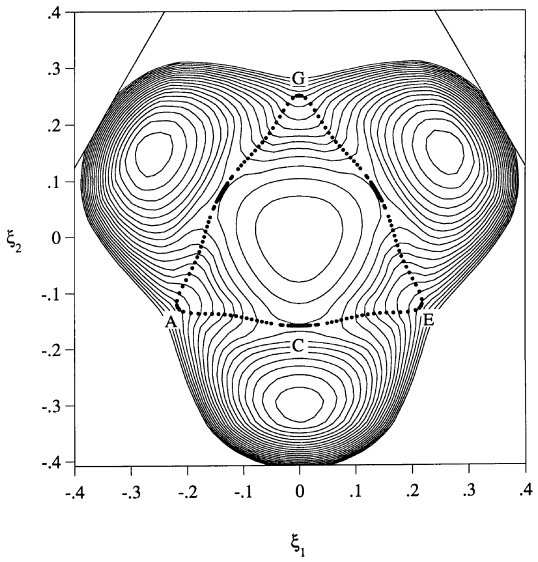

Fig. 9. Projection of the intersection seam, given by Figs. 5 and 6, onto the contours of the ground state in the plane r = 4.6. Energy increment between contours = 10 mh

of C_s, while the A_2 and B_1 irreps of C_{2v} correspond to the A″ irrep of C_s.

Since the original crossing at point C, in C_{2v} symmetry, was between the 1^1A_1 and 2^1A_1 states, these two states become the states $1^1A'$ and $2^1A'$ when the seam enters C_s symmetry. However, upon return to C_{2v} symmetry at point A, *only one of the two states is found to return to* $^1A_1$*; the other turns out to become* $^1B_2$. At this point A, the intersection is thus *not* between two states of *like* symmetry, but between two states of *different* symmetry.

Since the off-diagonal element H_{12} between the diabatic states vanishes automatically between two such states, there exists only *one* crossing condition, namely $\Delta H = 0$ [see sentence after Eq. (8) above]. Since the C_{2v}-restricted molecule has two degrees of freedom, the

intersection subspace between $^1A_1$ and $^1B_2$ in C_{2v} is therefore of dimension $2-1=1$ (see Ref. [3]). Hence, there exists *another one-dimensional intersection seam* between the states we are considering, a seam that is constrained to lie entirely in C_{2v}, and also passes through point A. The seam in C_s which was displayed in Fig. 5 must then connect with this C_{2v}-constrained seam at right angles at point A. This is confirmed by Fig. 10, which shows contours of the energy difference between the 1^1A_1 and the 1^1B_2 states in the C_{2v} plane near point A. The dashed contours indicate where 1^1B_2 is lower in energy and the solid contours indicate where 1^1A_1 is lower. The solid line is the intersection seam between the two states in C_{2v}. The large dot marks the point A where the intersection seam, which we determined in C_s, extrapolates to the C_{2v} coordinate plane. It is seen to fall exactly on the independently determined $^1A_1-{}^1B_2$ intersection seam.

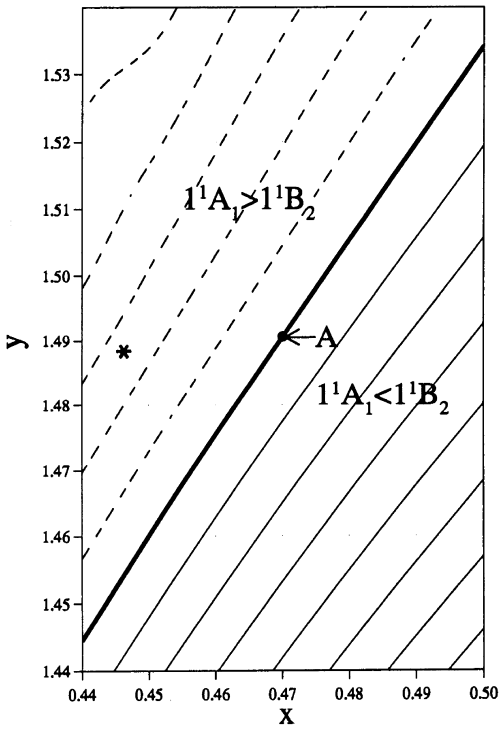

Fig. 10. Contours of the energy difference [E(1^1B_2)-E(1^1A_1)] in the C_{2v} restricted coordinated space near point A. The internal coordinates are the Cartesian coordinates of the end atom (see Fig. 3 of ref. [1]). Energy increment = 10 mh. *Solid lines*, >0; *dashed lines*, <0; *bold contour* = 0 = intersection seam in C_{2v}. The *dot* indicated as A is the point where the intersection seam given by Figs. 5 and 6 penetrates this *x*-*y* plane. *Asterisk*: see Sect. 4.5

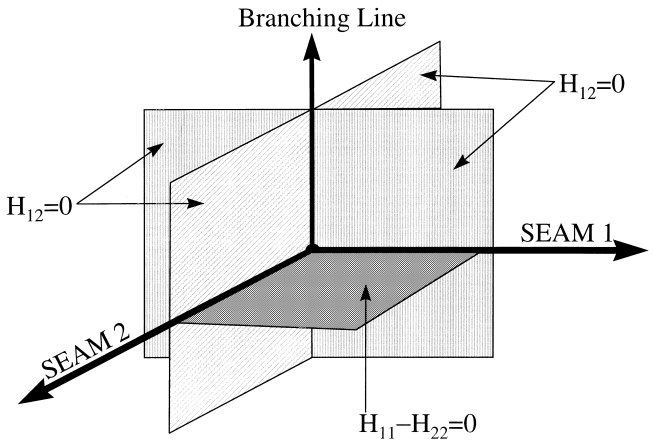

Fig. 11. Intersection seams near the confluence point A. H_{11}, H_{22}, H_{12} are matrix elements between diabatic states

4.4 The intersection node

We call the confluence A of the two seams a node. Here the standard dimensionality rules [3] regarding intersections require a modification which is readily understood in terms of the derivation of these rules (see, for example, our discussion in Ref. [3b]): In the present case we have, in the region of interest, *two surfaces* on which $H_{12}=0$ (one of them being the C_{2v}-conserving coordinate subspace) and one surface on which $H_{11}-H_{22}=0$, as illustrated in Fig. 11. The intersection of all three of these two-dimensional surfaces is the node A. The degeneracy is maintained on the *two* lines (Seam 1 and Seam 2) where the surface with $H_{11}-H_{22}=0$ intersects with each of the two surfaces $H_{12}=0$. The degeneracy is lifted on the line where the two surfaces H_{12} intersect with each other, i.e the *branching line* [3b]. In moving away from the node A, the degeneracy is lifted (to first order) only in directions with a component along the branching line.

Nodes such as A may be called *semi-conical* in the following sense: *Any* plane containing the branching axis also containes one vector perpendicular to it. Along this vector, the degeneracy is preserved to first order and, in such a plane, the energy difference between the upper and the lower state has therefore the shape of an ellipsoidal "semi-cone" *with an opening angle of* 180° *in one direction*. This conclusion is clearly illustrated by the near-equidistant contours in Fig. 10. Such semi-conical intersection confluences have also been encountered by Kuntz et. al. [4], who furthermore showed that the concomitant degeneracy of the two lowest eigenvalues of the Hessian of $(E_1-E_2)^2$ requires special precautions in methods using such Hessians.

4.5 The phase theorem

Near intersection nodes such as A, the geometric phase theorem [3], pertaining to wavefunction changes on closed loops, also requires modification. The situation is most easily understood in terms of the reasoning discussed above in Section 3.3.

First, a *closed* loop necessarily crosses the surface $\Delta H=H_{11}-H_{22}=0$ an *even* number of times since the latter divides the space into two half spaces. In one of these, the diabatic state ϕ_1 is dominant, in the other the diabatic state ϕ_2 is dominant for a given adiabatic state ψ. Second, whenever the loop crosses a surface $H_{12}=0$, the coefficient of the *non-dominant* diabatic admixture changes its sign. It follows then that ψ will change sign, if and only if the loop satisfies two conditions:

(i) The loop crosses the surface $\Delta H = 0$ *at leat once*;
(ii) While on each side of the surface $\Delta H = 0$, the loop crosses the surfaces $H_{12} = 0$ an *odd* number of times.

In the space depicted by Fig. 11, it is obviously possible to construct loops which either satisfy both conditions or violate one or the other. A simple example of the latter kind would be any loop circling the node A in a plane containing A, but not containing any one of the three axes. No phase change will occur on such loops.

4.6 Complete intersection seam

It is obvious that entirely equivalent situations must exist in the other two C_{2v}-restricted coordinate spaces which are obtained through rotations by $\pm 120°$ around the x_3 axis. We have not explored the full extent of the intersection seam between the 1^1A_1 and 1^1B_2 states since it lies in a dynamically rather inaccessible region of the C_{2v} coordinate space. Two possibilities for these additional seams, viz. an open seam and a closed seam, are schematically sketched in Fig. 12. This figure displays all four branches of the entire seam: the branch in C_s is denoted by S_0, the three C_{2v} branches by S_1, S_2 and S_3.

4.7 Orbital interpretation of the symmetry change

The symmetry change of one of the two states from A_1 at point A of Fig. 5 to B_2 at point C can be understood by the following reasoning in terms of orbital stabilities.

In C_s, the FORS wave function is constructed from 12σ-type MOs, belonging to the irrep A', and 3π-type MOs, belonging to irrep A''. It is found that, along the entire seam and for both states, nine natural orbitals of A' symmetry (three core and six valence orbitals) maintain near-constant double occupancy, whereas two natural orbitals of this symmetry remain effectively empty throughout. In addition, one natural orbital of A'' symmetry maintains near-double occupancy along the entire seam. This leaves three orbitals whose occupancies vary significantly in going from point C to point A, namely

$$\sigma = |10a'\rangle, \quad \pi_1 = |2a''\rangle, \quad \pi_2 = |3a''\rangle.$$

Figure 13 exhibits plots of the three orbitals for three points along the seam. The σ orbitals are plotted in the molecular plane, the π orbitals in a plane above and parallel to the molecular plane. At further intermediate points, the analogous plots look similar. The orbital symmetries are also given in these plots. It may be noted that, because of a degeneracy in the occupation numbers in both states at point A (see below), the two π orbitals can be arbitrarily superimposed and, thereby, two orbitals similar to those at the intermediate point can be generated. (The orbitals plotted are the FORS optimized orbitals which are nearly identical with the natural orbitals).

In Fig. 14, we show the variations of the natural orbital occupation numbers along the seam in going from point C to point A. The label INT indicates the point on the seam to which the intermediate orbitals of Fig. 13 belong. The solid dots represent the natural orbital occupations of state 1, the hollow dots those of state 2. As was mentioned earlier, the calculated states are not exactly degenerate, but differ by about 0.5 μh. This difference is sufficient to maintain the character of the two wave functions so that the orbital occupations do follow non-erratic, continuous curves. We denote the lower state as "state 1" and the higher state as "state 2".

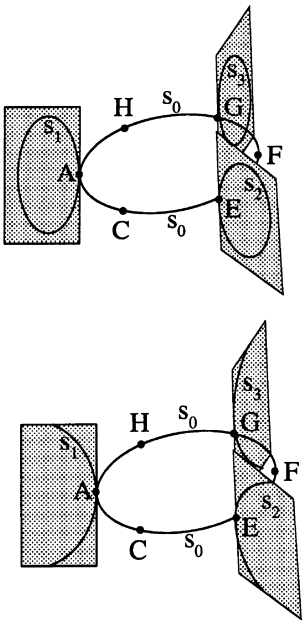

Fig. 12. Two possibilities for the four branches of the $1^1A'$-$2^1A'$ intersection seam in the shape-scale coordinate space. *Shaded planes*, C_{2v}-restricted coordinate regions

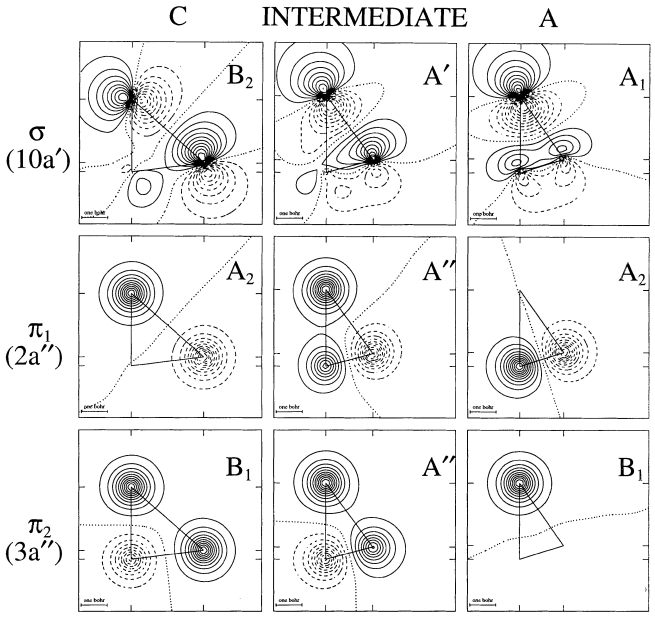

Fig. 13. Natural orbitals of ozone at three points along the seam from point C to point A. *Contours of σ orbitals*, in a molecular plane *contours of π*, in a plane above and parallel to molecular plane

For state 1, one recognizes the following occupation changes. In going from point C to point A, the orbitals π_1 and π_2 each lose one electron and both electrons go into the orbital σ. The presumed reason is that σ manifestly changes from an anti-bonding to a bonding orbital, whereas the π_1, π_2 set changes from slightly anti-bonding to more strongly anti-bonding. State 2 exhibits a compensating charge shift in the opposite direction which is attributable to the maintenance of orthogonality between the two states.

The coefficients of the dominant configurations of both states are listed in Table 2. It is seen that the single occupation of orbitals π_1 and π_2 in state 1 at point A result from a configuration in which both these orbitals are singly occupied so that the wave function of state 1 belongs indeed to the irrep $A_2 \otimes B_1 = B_2$. At point C it manifesty belongs to the irrep A_1. State 2, however, has only dominant configurations with doubly occupied orbitals throughout, so that it always belongs to the irrep A_1.

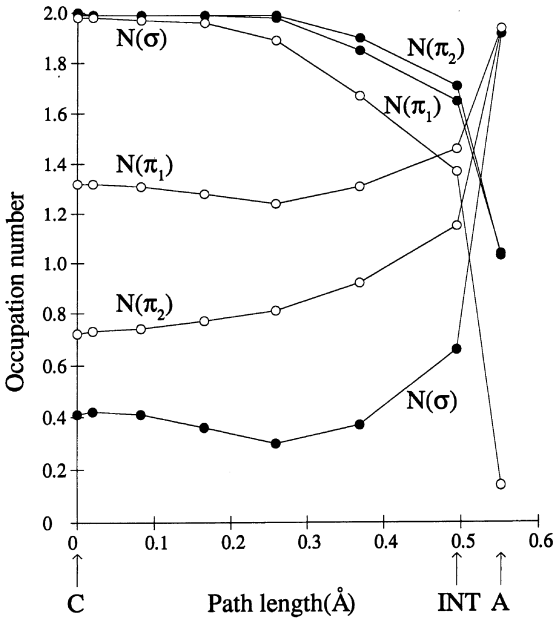

Fig. 14. Occupation numbers of the natural orbitals σ, π_1, π_2 along the $1^1A'$-$2^1A'$ intersection seam from point C to point A. *Solid dots*, occupancies for state 1; *hollow dots*, occupancies for state 2

Table 2 Dominant configurations of the $1^1A'$ and $2^1A'$ states

Configuration	Point C		Point A	
	State 1	State 2	State 1	State 2
$(\text{Core})^a\sigma^0\pi_1^2\pi_2^2$	−0.85	−0.02	0.00	0.93
$(\text{Core})^a\sigma^2\pi_1^2\pi_2^0$	0.01	0.75	0.00	0.00
$(\text{Core})^a\sigma^2\pi_1^0\pi_2^2$	0.04	−0.54	0.00	0.00
$(\text{Core})^b\sigma^2\pi_1^2\pi_2^2$	0.41	0.00	0.00	0.00
$(\text{Core})^a\sigma^2\pi_1^1\pi_2^1$	0.00	0.00	0.93	0.00

[a] (Core) = 11 doubly occupied σ-type orbitals and one doubly occupied π-type orbital
[b] (Core) = 10 doubly occupied σ-type orbitals and one doubly occupied π-type orbital

4.8 Another intersection seam of the 1^1A_1 *state*

In the course of the present work it was noticed that, in the C_{2v}-restricted space near the point A, the state 1^1A_1 comes very close to another $^1A_1$ state. Since, *at this point in the* C_{2v} *subspace*, the 1^1B_2 surface is lowest in energy, it is in fact part of the $1^1A'$ surface of the overall C_s symmetry, whereas the 1^1A_1 state (of C_{2v} symmetry) becomes $2^1A'$ in C_s notation. The new state is therefore $3^1A'$. Minimization of ΔE^2 and use of the Herzberg–Longuet-Higgins–Berry phase-change theorem proved that these two states of like symmetry ($1^1A_1 = 2^1A'$ and $2^1A_1 = 3^1A'$), too, intersect in C_{2v} symmetry. This point is marked with an asterisk in Fig. 6. It lies approximately 25 mh higher in energy than the intersection point A. From the general dimensionality rules it follows that another one-dimensional intersection seam involving the $2^1A'$ and $3^1A'$ states may exist, leading into C_s symmetry from this new intersection point.

5 Conclusions

The intersection seam between the lowest two $^1A'$ states of ozone has a multi-connected structure. It consists of four branches S_0, S_1, S_2, S_3 which are connected through four knots, as illustrated in Fig. 12. The knots and the three C_{2v}-restricted branches S_1, S_2, S_3 lie, however, in a highly repulsive part of the PES. The S_0 branch cuts through C_{2v} symmetry at two kinds of points. At the low-energy C_{2v} points both states have $^1A_1$ symmetry, but, at the high-energy C_{2v} points (the knots) one state has $^1A_1$ symmetry and the other has $^1B_2$ symmetry. This change is due to changes in orbital stabilites along the seam.

However, a large part of the branch S_0 in C_s symmetry lies at relatively low energies and, thus, offers ample opportunity for radiationless transitions (see Fig. 8). Hence, a discussion of such transitions, taking into account solely the minimum on the intersection seam (as is occasionally proposed), will manifestly yield an inadequate analysis. Furthermore, we shall show elsewhere [14] that the seam is imbedded in a region where the energy difference between $1^1A'$ and $2^1A'$ is small.

Intersections with further surfaces exist.

The method of "corralling an intersection" deserves further attention. It is based on identifying the curves on which the *diabatic* energy functions ΔH and H_{12} vanish by means of monitoring the sign and magnitude changes of the dominant coefficients of the *adiabatic* states.

Acknowledgements. This work was supported by the Division of Chemical Sciences, Office of Basic Energy Sciences, US Department of Energy (USDOE). The Ames Laboratory is operated for the USDOE by Iowa State University under Contract no. W-7405-Eng-82.

References

1. Xantheas S, Atchity GJ, Elbert ST, Ruedenberg K (1991) J Chem Phys 94:8054
2. Atchity GJ, Ruedenberg K (1993) J Chem Phys 99:3790

3. (a) Herzberg G, Longuet-Higgins HC (1963) Discuss Faraday Soc 35:77; Berry MV (1975) Proc R Soc Lond A 344:147; Mead CA (1979) J Chem Phys 70:2276; Mead CA, Truhlar DG (1979) J Chem Phys 70:2284 (b) Atchity GJ, Xantheas SS, Ruedenberg K (1991) J Chem Phys 95:1862
4. Kuntz PJ, Whitton WN, Paidarova I, Polak R (1994) Can J Chem 72:939
5. James HM, Coolidge AS (1937) Phys Rev 51:855
6. Pekeris CL (1958) Phys Rev 112:1649
7. Davidson ER (1977) J Am Chem Soc 99:397
8. Atchity GJ, Ruedenberg K (1997) Theor Chem Acc 96:205–211
9. Manaa MR, Yarkony DR (1990) J Chem Phys 93:4473; see also Koga N, Morokuma K (1985) Chem Phys Lett 119:371
10. Manaa M, Yarkony DR (1994) J Am Chem Soc 116:11444
11. Ragazos IN, Robb MA, Bernardi F, Olivucci M (1992) Chem Phys Lett 197:217
12. Dunning TH Jr (1989) J Chem Phys 90:1007
13. Werner HJ, Knowles PJ (1985) J Chem Phys 82:5053; Werner HJ, Knowles PJ (1985) Chem Phys Lett 115:259
14. Atchity GJ, Ruedenberg K (1997) Theor Chem Acc 96:176–194